Ultrasensitive Quantum-Limited Far-Infrared STJ Detectors

D. E. Prober, *Member, IEEE*, J. D. Teufel, C. M. Wilson, L. Frunzio, M. Shen, R. J. Schoelkopf, T. R. Stevenson, and E. J. Wollack

***Abstract*—We describe recent work at Yale on Superconducting Tunnel Junction (STJ) direct detectors that have been developed for submillimeter astronomy. To monitor the response of the detector with large readout bandwidth and excellent sensitivity, we use a novel readout based on radio frequency (RF) reflectometry, like the readout invented for the RF-SET. For calibration of the detector, we have developed an in-situ, on-chip, hot-cold photon source. This is a voltage biased gold microbridge. Noise emitted by the microbridge couples via a coplanar stripline to the detector. This provides a calibrated blackbody photon source with near unity coupling, fast chopping, and calculable output. We present recent detection results in the range 100–160 GHz. These demonstrate the expected good responsivity, high sensitivity, and fast response. This approach is easily used with a frequency-multiplexed readout, allowing economy of cold electronics. Ultimate sensitivity is in the range 1×10^{-19} W/(Hz)$^{1/2}$.**

***Index Terms*—Bolometers, submillimeter wave detectors, superconducting devices.**

I. Introduction

During the past decade, advances in superconducting thin-film technology have enabled the development of increasingly sensitive power detectors for observations in the mm-wavelength and sub-mm range. Bolometer detectors are read out with superconducting thermometers (TESs) and multiplexed SQUID amplifiers. These and other approaches are under development for current and future astronomy observations [1], [2]. Increasingly, thin film circuits allow for integration of the rf coupling and bandpass elements; sensitive SQUID readouts are on one or a few chips. One cited future application is the measurement of the Cosmic-Microwave Background (CMB) polarization anisotropy [3], [4]. Some future experiments, with cooled, space-borne collectors, may be able to utilize sensitivity values characterized by a Noise-Equivalent Power NEP $\approx 10^{-19}$ to 10^{-20} W/(Hz)$^{1/2}$. At this level, counting of individual photons may be possible, and has been predicted to be feasible with future developments [5], [6].

We describe here research at Yale University in collaboration with researchers at Goddard Space Flight Center. This work is to develop an extremely sensitive direct (power) detector for the mm and sub-mm wavelength region. The approach uses photoexcitation, the breaking of a Cooper pair into single-charge units by the absorbed photon. Our approach differs from those in which thermal excitations are created in a normal or gapless metal. The readout we have recently developed, a rf-resonant impedance transformer used in a measurement of reflection coefficient, allows frequency multiplexing of many single pixels to form a planar array. Moreover, the readout is very fast ($< \mu$sec) and simple to implement. Testing of any of the proposed devices at the low power level of the future applications, P $= 10^{-18}$ to 10^{-13} W, is very challenging. We have developed an on-chip photon source that allows testing with the photons that are in the mm-wave band, and can also be used easily with other device approaches. With these new techniques we have tested devices and demonstrated a NEP $< 10^{-16}$ W/(Hz)$^{1/2}$, limited by noise of the HEMT amplifier. With colder and smaller tunnel junctions and a lower noise (SQUID) amplifier, we expect this readout method will allow NEP $\approx 10^{-19}$ W/(Hz)$^{1/2}$. To achieve sensitivities that are even better, a RF-SET readout would need to be employed with this STJ detector [5]. The testing we have done has characterized the tunnel junctions and the general fabrication approach in a realistic model system, with all pieces functioning and integrated together. It lays the groundwork for tests of more sensitive devices in the future.

II. Detector and Readout Design

The device geometry is shown in Fig. 1 with a band diagram. The planar Nb antenna couples photons to the Al strip. A bowtie antenna is shown as an example, but other antenna types can be employed. For photon energies above the gap of Al ($E_{g,Al} = 2\Delta_{Al} \approx 100$ GHz) the photon is absorbed in the Al; each photon breaks a Cooper pair to produce two quasiparticles. These quasiparticles are at relatively low density and recombine slowly, on a timescale of msec [7]. The quasiparticles are confined to the Al strip by the larger gap Nb electrodes, and tunnel to the other Al electrode in a few μsec. With a finite voltage bias applied, the quasiparticles all tunnel as electrons [8] and a current flows proportional to the absorbed power P: I $= 2e$ (P/hf), with (P/hf) the number of photons absorbed at energies above E_g if the power is in a narrow band at frequency f. We assume that the resistance at frequency f of the Al strip matches the impedance of the antenna or the source

Manuscript received August 25, 2006. This work was supported by NASA and NASA-GSFC.

D. E. Prober, J. D. Teufel, L. Frunzio, M. Shen, and R. J. Schoelkopf are with the Department of Applied Physics and the Department of Physics, Yale University, New Haven, CT 06511 USA (e-mail: daniel.prober@yale.edu; john.teufel@yale.edu; luigi.frunzio@yale.edu; minghao.shen@yale.edu; robert.schoelkopf@yale.edu).

C. M. Wilson was with the Department of Applied Physics and the Department of Physics, Yale University, New Haven, CT 06511 USA. He is now with Chalmers University, SE-412 96 Göteborg, Sweden (e-mail: chris.wilson@mc2.chalmers.se).

T. R. Stevenson and E. J. Wollack are with the NASA GSFC, Greenbelt, MD 20771 USA (e-mail: thomas.r.stevenson@nasa.gov; edward.j.wollack@nasa.gov).

Color versions of Figs. 1–11 are available online at http://ieeexplore.ieee.org.

Digital Object Identifier 10.1109/TASC.2007.897397

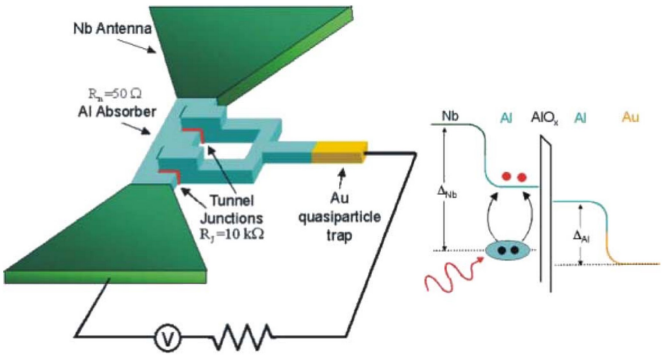

Fig. 1. Schematic of detector and band diagram.

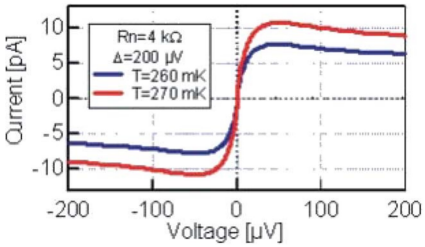

Fig. 2. I–V at low voltages versus temperature.

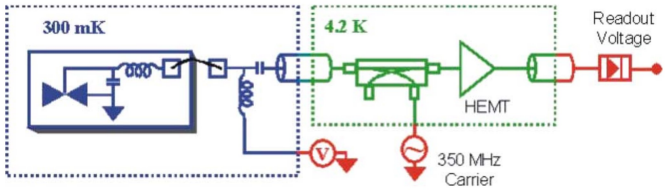

Fig. 3. Resonant readout method, as described in the text.

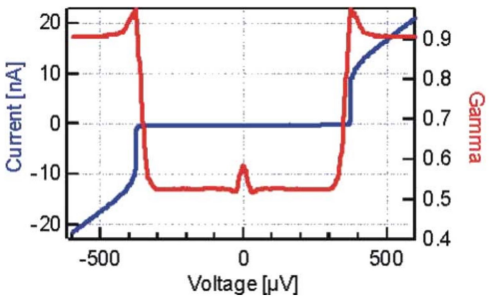

Fig. 4. I–V curve and reflection coefficient. Peak near $V = 0$ is due to the larger conductance seen in Fig. 1 near $V = 0$. This peak grows when the temperature or photon-induced current increases with increased absorbed power.

driving it, so all incident power is absorbed. With the Nb antenna, the frequency range for operation of this specific design is from 100 GHz to ≈650 GHz. (The Nb gap is slightly reduced in our thin film.) The Au quasiparticle trap ensures that the quasiparticles, after tunneling, leave the junction area rapidly by diffusion and cannot tunnel back to the Al absorber. The thermally excited quasiparticles give a dark current with current shot noise $= 2e|I_{dc}|$. This can typically be ignored for $T \leq 0.2$ K. We note that this dark current is given by the BCS prediction for the sub-gap current down to at least 150 mK [9].

Prior to photon testing we wanted to test the various readout methods and to better understand the junction fabrication issues. We first used tests of response vs. temperature, with the increase of BCS subgap current at higher temperatures modeling the effect of the induced current due to absorbed photons. In Fig. 2 we plot the I–V curves for two temperatures, the base temperature of that measurement, 260 mK, and a temperature 270 mK, only 10 mK higher. We see a current increase of 3 pA, measured with conventional room temperature dc instruments. (Cold rf filters are employed.) Such measurements confirm the ideal quality of the junctions, and also the suppression of the critical current. We use a magnetic field perpendicular to the plane of the junctions, which form a SQUID magnetometer. The individual small junctions are too small to suppress their critical current with a parallel field that is below $H_{c||}$ of the Al film.

The response speed of the 'dc' electronics is far too slow for most applications, due to the large junction resistance (> Mohm for $V > 20$ μV) combined with the cable capacitance to room temperature. A much faster readout method is offered by the resonant impedance transformation and rf reflection measurement developed for readout of the RF-SET [10]. We have further developed this technique, and describe it below. It offers the great advantage that one can frequency multiplex many individual detectors using a 'comb' of interrogating radio frequencies, each addressing one detector with its own resonant frequency. Only one cold amplifier and cable are required, with each detector of a planar array being read out simultaneously with all others, each having a bandwidth >1 MHz [11], [12].

Fig. 3 shows the resonant rf readout method. The Nb antenna is shown schematically. The impedance of the tunnel junction connects to the C-L circuit which is attached directly to it on the same chip. A wire bond connects this chip to the cold bias Tee, which allows one to dc bias the junction with a voltage V, and to pass rf signals at 350 MHz in this case through a large coupling capacitor. A cable connects to the directional coupler at 4.2 K. The rf signal is sent toward the tunnel junction, and the impedance of the junction "seen" at the wire bond is transformed down from the large (Mohm) value of the junction resistance to around 50 ohms. If the transformed impedance is exactly 50 ohms, there is no reflection, and if it differs from 50 ohms, the voltage reflection coefficient is either positive or negative. Thus, small changes of the tunnel junction impedance are sensed when one measures the reflected power. The reflection coefficient measured over the full I–V curve is shown in Fig. 4. The peak around $V = 0$ is due to the large conductance near $V = 0$, in Fig. 2.

The most sensitive detection will be achieved with small junctions at cold temperatures, ≤150 mK. We predict that our resonant rf readout can achieve a noise-equivalent power of NEP $\approx 1 \times 10^{-19}$ W/(Hz)$^{1/2}$ if we employ a SQUID rf amplifier instead of the HEMT amplifier that has been tested so far. This NEP corresponds to a power level $\approx 10^{-16}$ W, which would generate a background-limited NEP (due to photon shot noise) of this same level. This power corresponds to absorbing 150 GHz photons at a 1 MHz rate. This is the limit of sensitivity of the present readout method even with the SQUID rf amplifier. To achieve lower NEP values, one would need to employ a RF-SET readout [5], [10]. We have opted to avoid

that complexity in developing our understanding of junction dynamics and the materials issues and how they affect device performance, and instead used the resonant rf readout, Fig. 4. With this readout we learned how to conduct tests of NEP with mm-wavelength photons. We describe that next.

Testing the detector response with mm-wavelength photons can be challenging, especially if this is done in a quantitative fashion. We initially tested the antenna-coupled detector. We used a well characterized 200 GHz black-body source that radiated through a waveguide-horn combination [13]. We unfortunately did not achieve good rf coupling in the initial experiments, and opted instead to develop the on-chip black-body source. This allows very efficient coupling, near unity efficiency, and fast turn-on and turn-off. Moreover, it has an easily calculated spectrum which can produce photon power in the range 10^{-16} to 10^{-12} W in the millimeter band above the Al gap frequency, as needed for the tests envisioned.

The blackbody source we developed is a narrow (0.1 μm) gold wire, 0.5 μm long and about 20 nm thick; the resistance is near 50 ohms to match the transmission line. It is contacted on each end by a thick Au contact. When a voltage is applied, the wire heats up, and the electrons are in a regime where the electron temperature is defined, but varies with position x along the wire, being largest in the center. The dissipated power is removed by hot electrons flowing out of the wire, driven by the temperature gradient. This diffusion cooling is well known from work on hot-electron bolometer mixers [14], [15] and one can simply compute T(x) of the wire. To compute the power emitted into a matched load, we use the black-body emission formula for a resistor and integrate along the wire length the emitted power from each segment dx at T(x) at each specific frequency. The total power is just the frequency integral starting from $\mathrm{f} = \mathrm{E_{g,Al}/h}$. The total power per Hz coupled into a matched load, from a length dx at position x, is

$$\mathrm{P(x)/(Hz)} = \left\{ \mathrm{hf} / \left[\mathrm{e}^{(\mathrm{hf/kT(x)})} - 1 \right] \right\} \mathrm{dx/L}.$$

Here, L is the length of the Au wire, k is Boltzmann's constant, and h is Planck's constant. At low frequencies, P(x)/(Hz) from a length dx is kT(x)(dx/L). The total power emitted into a matched load is $\mathrm{k}\langle \mathrm{T(x)} \rangle / (\mathrm{Hz})$, with $\langle \mathrm{T(x)} \rangle$ the average electron temperature along L. Recall that $\mathrm{hf} = \mathrm{kT}$ for $\mathrm{f} = 20$ GHz and $\mathrm{T} = 1$ K. For average temperatures of 1 to 3 K, the power emitted is in the range <0.1 to 0.5 pW.

The photons emitted by the Au blackbody are coupled via a coplanar stripline (CPS) of design impedance 50 ohms to the Al strip, which absorbs photons of energy above $\mathrm{E_{g,Al}}$. The Al strip has normal state resistance ≈50 ohms, and at frequencies above the Al gap, the rf impedance is close to 50 ohms (see also below). The stripline has large SiO capacitors to block the dc bias of the Au wire, so the Al strip has no dc voltage across it. To make testing simple, we first used a relatively large single junction, of area 2.5 $\mu\mathrm{m}^2$. This allowed us to use the existing sample holder geometry, which has a magnetic field parallel to the substrate, to suppress the Josephson current. This suppression is needed for reliable biasing of the tunnel junction. A schematic of the test chip and rf readout is shown in Fig. 5. The

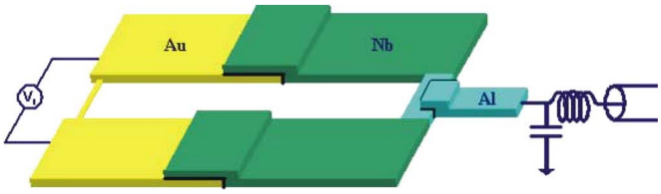

Fig. 5. Schematic of test chip with rf readout. Here, a single junction is used for convenience. Squid-geometry STJs have also tested well.

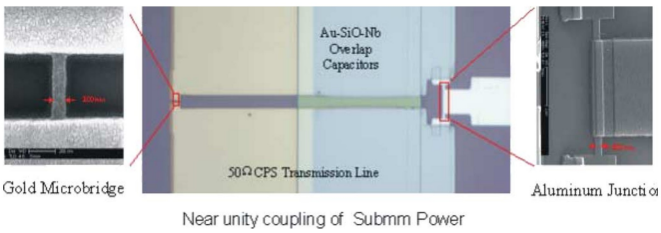

Fig. 6. Optical micrographs of finished device, with electron micrographs of the Au emitter and the tunnel junction. Schematic of the Au wire emitter. DC/Low frequency connections to the Au wire and to the tunnel junction are not shown.

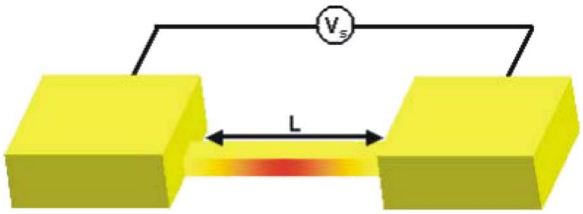

Fig. 7. Schematic of the Au wire.

entire structure is shown in optical and electron micrographs in Fig. 6. A schematic of the Au blackbody emitter is shown in Fig. 7. We have measured separately the average temperature of the Au wire with dc voltage bias, using GHz Johnson noise thermometry. The result matches the computed average temperature [15], [16]. We have also measured detectors in the SQUID geometry (Fig. 1) using the same transmission line geometry with Au emitter.

Recent tests have shown that some of the mm-wavelength photons may be lost by radiation into the SUBSTRATE when we employ a different layout. This is not a problem for the device and layout shown. Use of a co-planar waveguide (CPW) as the transmission line will give much more localized fields, and minimize possible emission of photons into the substrate. Many detector designs call for such a CPW feed; we used the CPS transmission line only as a first test. The low frequency connections, not seen in Fig. 6, are narrow and widely spaced, and are designed to have much higher impedance. This prevents leakage of the mm-wavelength photons out these connections. Designed choke structures could be used. These would need to be fairly broadband for the large frequency range used in these tests.

III. Experimental Results

Detector I–V curves for various levels of emitter power are shown in Fig. 8. The temperature listed is the average for each computed T(x) distribution. The junction resistance in this case

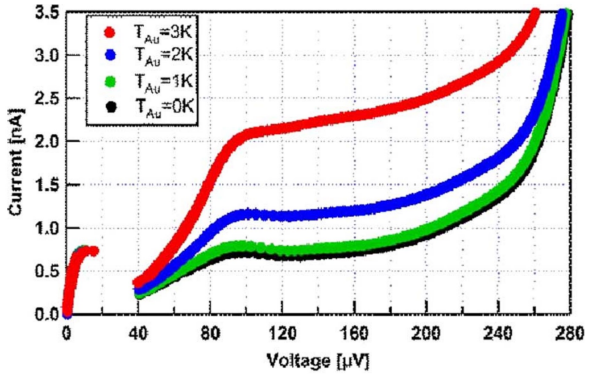

Fig. 8. I–V curves for four average temperatures of the Au wire emitter.

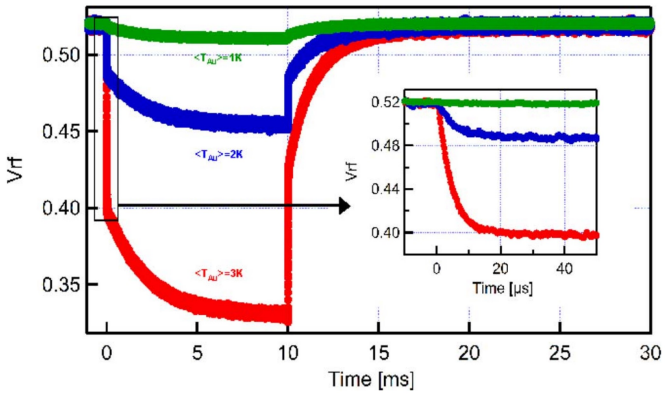

Fig. 9. Rf reflection with ≈100 Hz square wave heating the Au emitter. The fast (μsec) response is due to the photon-induced current. The much slower (5 msec) response is due to substrate heating, as outlined in the text.

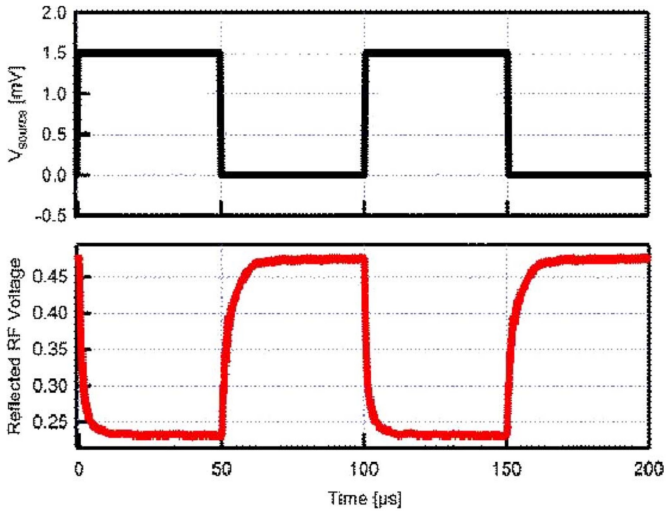

Fig. 10. Response of detector to a 10 kHz on-off square wave applied to the Au emitter. The response due to absorbed photons only is given by the peak-to-peak amplitude of the resulting output signal.

was $\mathrm{R_n} \approx 1$ kohm, lower than small, SQUID-type junctions that have also been tested in the two-junction SQUID geometry, Fig. 1. The base temperature of the measurement was 260 mK. These I–V curves have structure between 0 and 40 μV, unlike those of Fig. 3, due to the difference in energy of the gaps of the two Al electrodes. The higher gap electrode of the absorber was evaporated more slowly, to ensure that its resistance was ≈50 ohms. More recent tunnel junctions were produced with Al films that had nearly identical gap values. While the I–V of Fig. 8 appears more complex that the curves of Fig. 3, the rf readout still operates to distinguish the increase in current due to absorbed photons. We use a level of rf drive such that the junction voltage gets to ≈ 140 μV at its peak amplitude.

We checked the speed of the response by modulating the voltage across the Au wire with an on-off square wave. We measured with square waves of different amplitudes. What we found is shown with a ≈ 100 Hz square wave drive. As seen in the inset of Fig. 9, the fast response of the reflected rf voltage follows the input power with a time constant of a few μsec, which is the response time of the quasiparticle tunneling current. This is the expected result, since the tunnel time is expected to be the limiting time for junction response to absorbed mm-wave photons. The rf readout itself is much faster, being able to follow changes of emitted power on a 0.1 μs scale. The blackbody emitter turns on and off even faster, with a time constant set by diffusion along its short length; we estimate this time constant to be ≤ 0.1 nsec. The quasiparticles in the Al absorber cool to near the gap in less than a μsec [8].

When we view the measurement of Fig. 9 on a msec time scale (main plot), we observe a second behavior. We see a second time constant where the response slowly approaches its full value. There is a fast initial transition on the μsec scale due to the response to absorbed photons, seen in the inset, but then a very slow approach to the final value, on the scale of 5 msec. We have identified this slow response as due to substrate heating. There are two pieces of strong evidence. First, a second detector on the same chip, not connected to the heated black body emitter, shows only the slow response, and of a nearly similar magnitude as the detector that is connected by CPS to the emitter. Second, when we later used multiple wirebonds from Au pads on top of the substrate to the copper frame, this slow heating effect was significantly reduced. We thus conclude that the measurement of the rf reflection on the fast timescale indicated the photon-induced change in quasiparticle current and resistance. We thus find that by using a 10 kHz square-wave drive for the voltage across the Au wire, we can observe just the desired response due to absorbed photons. This square-wave response is shown in Fig. 10. The slow response seen in Fig. 9, and a fraction of the dc response seen in Fig. 8, is due to the substrate heating. We have thus corrected the measured dc values of the current change of Fig. 8, and report the value of the responsivity with the substrate heating effect removed. We find this responsivity is $R = 1700$ A/W, which compares reasonably well to the predicted value of 3000 A/W. The predicted value was computed by accounting for the actual black-body spectrum presented to the absorber, and also the true impedance of the absorber at frequencies above the gap of Al. The impedance of the Al strip above its gap frequency differs slightly from the normal state resistance $\mathrm{R_n}$ due to the BCS electrodynamics [17]. We used the Mattis-Bardeen theory for this computation. We do not have a firm explanation of the difference between the predicted and observed values of the

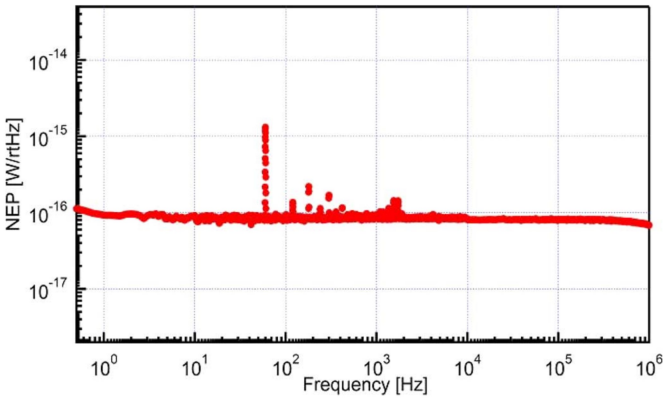

Fig. 11. NEP of the detector as a function of frequency.

responsivity. However, we note that the overall agreement and performance are very encouraging.

The optical NEP of our detector is shown in Fig. 11. This is for measuring with absorbed photons. We use the responsivity from the reflection measurement with the 10 kHz drive of the Au emitter. We measured the noise while the detector was operating under load. The noise was found to be white down to about 1 Hz, as shown in Fig. 11. The value of the NEP for intermediate frequencies is 8×10^{-17} W/(Hz)$^{1/2}$. This value of NEP is very close to that predicted solely on the basis of the amplifier noise and the Q factor of the resonant circuit used, Q $\approx$ 20. To achieve the much lower values of NEP that this detector should be able to provide, one would use smaller junctions (i.e., two junctions of total area ≤ 0.1 μm^2, in a SQUID geometry) and much lower temperatures. These changes, taken together, would dramatically lower the dark current and thus give much larger tunnel junction resistance hear V $= 0$. In turn this would allow for Q values one to two orders of magnitude larger, reducing the current noise referred to the tunnel junction by that same ratio. These low dark currents were demonstrated in past dc measurements, where dark currents $= 10$ fA were observed [16]. With a SQUID rf amplifier, a NEP of 1×10^{-19} W/(Hz)$^{1/2}$ is predicted [18].

We emphasize that we measure and report an optical NEP, which is often a very challenging goal for this mm-wavelength range of detection. For many thermal detectors, the electrical NEP is what is reported, or the computed NEP based on a measurement of thermal conductance. Our on-chip source allows the optical NEP to be measured. Careful thermal design can make the substrate (phonon) heating effects negligible.

IV. Conclusion

A conclusion of this work is that reliable testing of mm-wavelength and sub-mm systems can benefit from using on-chip sources of photons that produce a known spectrum and power in the cryogenic environment. While the use of a blackbody source in the cryogenic environment is over 20 years old [19], [20], our use of an on-chip blackbody in this millimeter frequency range appears to be new, and is very useful. We have identified some of the potentially complicating issues, such as substrate (phonon) heating, and shown how to remove these as impediments. While the goal of achieving good coupling to photons arriving from free space, for astronomy observations, needs to also be implemented, the development of an on-chip test system with fast response provide a useful tool during development of these future astronomy systems.

Acknowledgment

The authors thank A. Szymkowiak, J. Zmuidzinas, B. Karasik, and R. McGrath for useful discussions, and J. Chudow for assistance.

References

[1] Proceedings of the LTD Conference. Tokyo, Japan, Aug. 2005.
[2] *Nuclear Instruments and Methods A*, vol. 55, 2006.
[3] J. T. Skidmore, J. Gildemeister, A. T. Lee, M. J. Myers, and P. L. Richards, "Superconducting bolometer for far-infrared Fourier transform spectroscopy," *Appl. Phys. Lett.*, vol. 82, pp. 469–471, 2003.
[4] T. R. Stevenson, W.-T. Hsieh, G. Schneider, D. Travers, N. Cao, E. Wollack, M. Limon, and A. Kogut, "Building blocks for a polarimeter-on-a-chip," *Nuclear Instruments and Methods in Physics Research. A*, vol. 559, pp. 611–613, 2006.
[5] R. J. Schoelkopf, P. Wahlgreen, A. A. Kozhevnikov, and P. Delsing, *IEEE Trans. Appl. Supercond.*, vol. 9, pp. 2935–2939, 1999.
[6] B. S. Karasik and A. V. Sergeev, "THz hot-electron photon counter," *IEEE Trans. Appl. Superconductivity*, vol. 15, pp. 618–621, 2005.
[7] C. M. Wilson, L. Frunzio, and D. E. Prober, "Time-resolved measurements of thermodynamic fluctuations of the particle number in a nondegenerate Fermi gas," *Phys. Rev. Lett.*, vol. 87, pp. 067004-1–067004-4, 2001.
[8] K. S. Segall and D. E. Prober, "Quantum partition noise in superconducting tunnel junctions," *Phys. Rev. B, Rapid Commun.*, vol. 64, pp. 18058-1–18058-4, 2001.
[9] V. Savu, Ph.D. thesis, Yale Univ, New Haven, CT, Dec. 2006.
[10] R. J. Schoelkopf, P. Wahlgren, A. A. Kozhevnikov, P. Delsing, and D. E. Prober, "The radio-frequency single-electron transistor," *Science*, vol. 280, pp. 1238–1242, May 1998.
[11] T. R. Stevenson, F. A. Pellerano, C. M. Stahle, K. Aidala, and R. J. Schoelkopf, "Multiplexing of radio-frequency single-electron transistors," *Appl. Phys. Lett.*, vol. 80, pp. 3012–3014, 2002.
[12] D. E. Prober, J. D. Teufel, L. Frunzio, C. M. Wilson, and R. J. Schoelkopf, "Quasiparticle dynamics and a new, high-resolution readout of STJ photon detectors," *Nuclear Instrum. Methods Phys. Res. A*, vol. 559, pp. 676–679, 2006.
[13] E. Wollack, *Goddard Space Flight Center.* private communication and unpublished.
[14] D. E. Prober, "Superconducting terahertz mixer using a transition-edge microbolometer," *Appl. Phys. Lett.*, vol. 62, p. 2199, 1993.
[15] P. J. Burke, R. J. Schoelkopf, D. E. Prober, A. Skalare, B. S. Karasik, M. C. Gaidis, W. R. McGrath, B. Bumble, and H. G. LeDuc, "Mixing and noise in diffusion and phonon cooled superconducting hot-electron bolometers," *J. Appl. Phys.*, vol. 85, p. 1644, 1999.
[16] J. D. Teufel, Ph.D. thesis, Yale Univ., New Haven, CT, unpublished.
[17] M. Tinkham, *Introduction to Superconductivity*, 2nd ed. New York: McGraw Hill, 1996.
[18] D. E. Prober and T. R. Stevenson, unpublished.
[19] D. W. Face, D. E. Prober, W. R. McGrath, and P. L. Richards, "High quality tantalum superconducting tunnel junctions for microwave mixing in the quantum limit," *Appl. Phys. Lett.*, vol. 48, p. 1098, 1986.
[20] W. R. McGrath, Ph.D. thesis, UC Berkeley, Berkeley, CA, 1986.